FATIGUE BEHAVIOUR OF WELDED ALUMINIUM ALLOY JOINTS AT VERY HIGH CYCLES

M. Cremer, M. Zimmermann, H.-J. Christ
Institut für Werkstofftechnik
Lehrstuhl für Materialkunde und Werkstoffprüfung
Universität Siegen, 57068 Siegen, Germany

ABSTRACT

The aim of the present study is to investigate the behaviour of welded aluminium joints in the very high cycle fatigue (VHCF) range, focusing on a better understanding of the damage mechanisms. In this work the precipitation hardening alloy EN AW-6082 (AlMgSi1) and the work hardened alloy EN AW-5083 (AlMg4,5Mn) are analysed emphasising the fatigue behaviour of the base metal by means of notched and unnotched heat treated samples representing a MIG welded structure with a filler metal S Al-5183 (AlMg4,5Mn0,7). The weldments were prepared as double-V seams. After a detailed characterisation of the weld seam, cylindrical specimens of similar hardness and microstructure as the different welding zones were produced and used for fatigue tests. First results of the fatigue behaviour of these samples in the VHCF range are presented and discussed in this contribution, showing that for very high number of cycles the geometrical notch effect is not solely dominating the cyclic strength.

KEYWORDS

Aluminium welding, notch effect, very high cycle fatigue, ultrasonic fatigue testing, damage mechanism

INTRODUCTION

Welded aluminium joints are known to be used in structural components in many areas, e. g. in the aircraft, railway or automotive industry. The knowledge about the fatigue behaviour of such welding structures is an important, current and appealing issue and an important prerequisite for a safe life design. When discussing the fatigue behaviour of materials in the very high cycle regime current research work focuses on the damage mechanisms provoking crack initiation even at macroscopically purely elastic strains [1].

In case of welded joints these considerations depend on many different parameters e.g. macroscopic notches, microscopic notches in form of weld imperfections and microstructure discontinuities as well as strength gradients each of which could cause different damage mechanisms. Typically observed fatigue behaviour of aluminium alloys at higher number of cycles (approximately $N > 7 \cdot 10^6$) shows crack initiation both at the surface as well as in subsurface regions related to microstructural defects [2, 3].

As a consequence, crack initiation at micro- as well as macrostructural discontinuities acting as stress raisers must be analysed in order to specify the dominating mechanism. In this

respect Zhu et al. [4] described the fatigue behaviour of a 319 cast aluminium alloy in the gigacycle regime. The fractographic studies indicated that most fatigue cracks initiate from microshrinkage pores located at or very near to the specimen surface, while a smaller number initiate from interior features and planar grain or twin boundaries.
Studies of the fatigue behaviour of various aluminium alloys using an ultrasonic testing system showed a further increase of the scattering in the VHCF area [3, 4]. With the given increase in fatigue life scattering due to local microstructure-dependent stress raisers, the precise characterisation of the VHCF behaviour of welded structures implies a detailed characterisation of the weld geometry, of typical weld inhomogeneities such as e.g. hot cracks, pores, slag inclusions and of the structural notch of the different welding zones, resulting from the different temperature time histories of the heat gradient and transitions during the welding process. For a better understanding of the dominating damage mechanisms in the VHCF regime, those inhomogeneities have to be evaluated separatively, thus identifying the crucial (process) parameters to decrease the scattering of the fatigue results.

MATERIAL AND EXPERIMENTAL PROCEDURE

The materials used in this study are the precipitation hardening aluminium alloy EN AW-6082 (AlMgSi1) and the work hardened aluminium alloy EN AW-5083 (AlMg4,5Mn). With their high tensile strength, which is competitive to structural steel, both materials are mainly used for highly stressed structural parts in many different industrial sectors e.g. automotive or railway applications. Two batches of EN AW-6082 with approximately the same chemical composition and as-received heat treatment condition were analysed in this study. A detailed listing of the mechanical properties and the chemical compositions of both alloys are given in table 1 and table 2, respectively. Figure 1 (a) and (b) depicts micrographs of the typical microstructure of the alloys in the as-received condition.

	Tensile strength [Mpa]	**Yield stress [Mpa]**	**Elongation [%]**	**Vickers hardness HV1**
EN AW-6082 T6 batch A & B (extruded material)	380	320	11	112
EN AW-5083 H111 (rolled blanks)	305	158	21	85

Table 1: Mechanical properties of the base metals used for the welded joints.

EN AW-6082* elements	**Mg**	**Mn**	**Si**	**Fe**	**Zn**	**Cu**	**Cr**	**Ti**	**Al**
Mass-%	0,6-1,2	0,4-1,0	0,7-1,3	0,5	0,2	0,1	0,25	0,1	Rest

(Single values are maximum content) ***chemical composition for batch A and B**

EN AW-5083 elements	**Mg**	**Mn**	**Si**	**Fe**	**Zn**	**Cu**	**Cr**	**Ti**	**Others**
Mass-%	4-4,9	0,4-1	0,4	0,4	0,25	0,1	0,05-0,25	0,15	0,15

(Single values are maximum content)

Table 2: Chemical compositions of the base metals used for the welded joints.

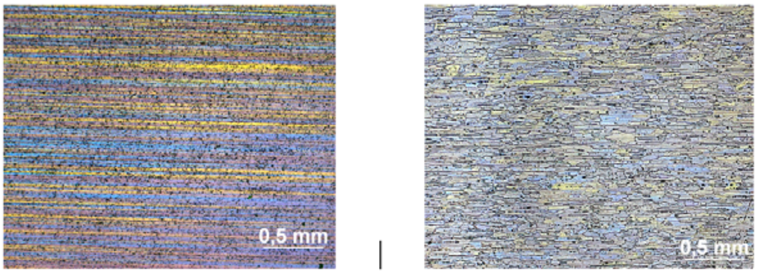

EN AW-6082 extruded **EN AW-5083 rolled**

Fig. 1: (a) Microstructure of EN AW-6082 (batch A) and (b) EN AW-5083.

Welded joints were manufactured focusing on a reproducible quality of the double–V butt weld seam from 6 mm rolled metal for both aluminium alloys. The joints were realized by using a microprocessor controlled pulsed MIG power source with a cooled welding torch and a controlled linear positioning welding bench, the cover gas was argon. In order to minimize the possible welding imperfections, the welding parameters were iteratively optimised and documented. The fatigue samples representing the base metal EN AW-6082 used in this study were heat treated at a temperature of 540°C for 40 minutes and in a second step reheated at 160°C for 60 minutes to establish the peak-aged condition (T6). Preliminary studies of the VHCF behaviour of 6082 in different heat treated conditions can be found elsewhere [5]. The geometries of the fatigue specimens shown in figure 2 were produced from extruded material of EN AW-6082 T6 and rolled blanks of EN AW-5083 H111. Both geometries were manufactured in the surface qualities as-machined and electrochemically polished.

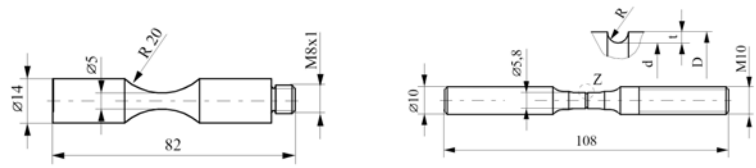

Type I for ultrasonic fatigue system Type II for servo-hydraulic system

Fig. 2: Geometry for fatigue specimens.

The specimens used for the ultrasonic fatigue system exhibit a cross-section of 5 mm in the critically loaded section. The notched specimens tested by means of a servo-hydraulic system featured a circumferential notch with a root radius (R) of 0.5 mm and a depth (t) of 1 mm, thus representing a similar notch effect as the welded blanks. To define the static notch factor two methods were used, the Collins diagram [6] and the analytical formula from the Forschungskuratorium Maschinenbau (FKM) e.V. guideline [7]:

$$K_t = 1 + \frac{1}{\sqrt{0{,}22 \cdot \frac{R}{t} + 2{,}74 \cdot \frac{R}{D} \cdot \left(1 + 2 \cdot \frac{R}{d}\right)^2}} \qquad (1)$$

The ultrasonic fatigue testing was carried out at a frequency of around 20 kHz by means of displacement control in intermittend pulse/pause sequences of 600 msec and 300 msec, respectively. In case of a fatigue crack initiation a decrease of the test frequency of 300 Hz was chosen to automatically stop the test. The notched specimens were tested load-controlled by means of a servo-hydraulic system at a frequency of 760 Hz. Tests ended with the fracture of the sample. All fatigue tests were realized at a stress ratio R = -1 and at room temperature (guaranteed by means of active cooling). The microstructures, weld inhomogeneities and fracture surfaces were characterized by means of optical and scanning electron microscopy (SEM). Vickers microhardness measurements for the different weld zones as well as the heat treated base metal were realised by using a Struers Duramin hardness tester.

RESULTS AND DISCUSSION

In order to specify the macroscopic notch of the weld seam eleven different polished micrograph sections of the double–V butt weld for optimized welding process parameters were measured and statistically analysed. Table 3 shows the minimum and maximum range of the geometrical parameters of the welded structures.

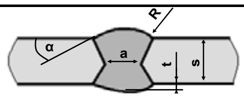	**R = 0,5-0,6mm**	**t = 0,9-1,1mm**	**a = 3,6-3,8mm**	**s = 6mm**	**α = 28-39°**

Table 3: Macroscopic geometry of the weld seam in the optimized condition.

Based on the notch geometry the static notch factor K_t was calculated according to [8, 9]

$$K_t = 1 + 0{,}27 \cdot (\tan\alpha)^{0{,}25} \cdot (\frac{t}{R})^{0{,}5} \qquad (2)$$

Hence, a range for the static stress concentration factor of K_t=1,798-1,809 was determined for the welded structures. These true values for the worst case macroscopic notch of the weld seam are in good agreement with the artificially notched fatigue specimens with $K_{t(Collins)}$=1,820 according to the Collins diagram and are slightly overestimated by the FKM guideline $K_{t(FKM)}$=2,445. Figure 3 shows the microstructure of the different weld zones: the heat-affected zone, the weld seam and the base material. Typical weld inhomogeneities such as e.g. hot cracks, pores, slag inclusions and incomplete fusions are indicated by white arrows. Future research work will focus on fatigue crack growth specimens, representing these defects and thus allowing a comparison with so far observed VHCF behaviour for aluminium alloys with defects, e.g. the work by Zhu et al. [4]. The question will be addressed, whether similar damage mechanisms can be observed for each constellation.

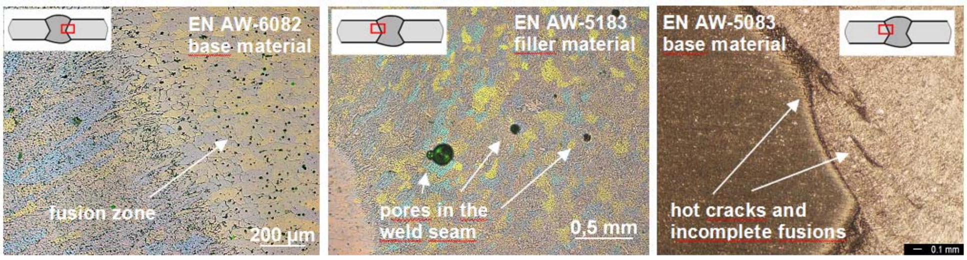

Fig. 3: Microstructure and typical inhomogeneities of the weld seam (a) fusion zone (b) pores in the weld seam (c) hot cracks and incomplete fusions

The structural notch effect along the weld seam was characterised based on the measurement of strength gradients by means of Vickers microhardness shown in figure 4. This notch effect deriving from the different sensitivities of the two alloys (a precipitation

hardening and a solid solution hardening alloy) to the concentrated heat input during the welding process leads to a strength mismatch and thus an unsymmetrical notch effect.
In general a weld seam is divided into three zones, the weld seam, the heat affected zone (HAZ) and the base metal. In the given study a more precise distinction is made according to the hardness of the EN AW-6082 welded material. The beginning of the heat affected zone (also called the fusion zone) shows a hardness of 85 HV, followed by a decrease of the hardness to 70 HV at 6 mm distance from the fusion zone. The original 112 HV hardness of the base material is given at a distance of 26 mm from the fusion zone, thus indicating the end of the heat affected zone. The welded structure of the EN AW-5083 alloy shows a constant hardness of 85 HV. The hardness of around 112 HV was also achieved by the heat treatment of the fatigue specimens of batches A and B for EN AW-6082.

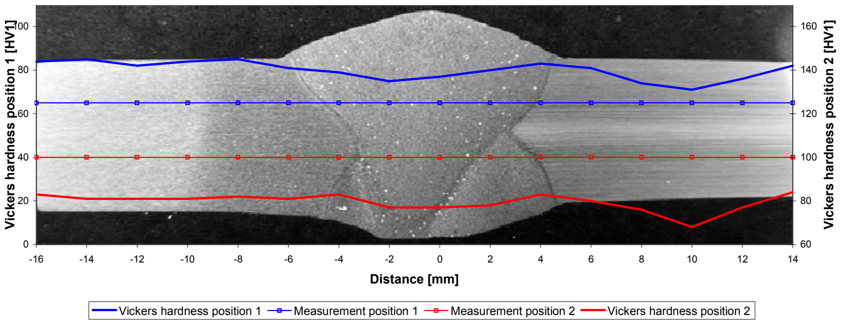

Fig. 4: Vickers hardness of a weld seam EN AW-5083 – EN AW-6082 (hybrid).

Figure 5 depicts the S-N data for the notched specimens of the EN AW-6082 alloy in the peak aged base metal condition. Arrows are used to indicate run-out specimens. The dashed lines only serve as a better visualization of the fatigue behaviour trends and do not yet represent a final S-N curve. An interesting effect is given by a comparison of the fatigue results for the two different batches of EN AW 6082. Despite a similar notch geometry, surface quality and hardness given for both batches, batch A shows a much higher cyclic strength in the VHCF regime than batch B. Future experiments will focus on the influence of the microstructure, e.g. the difference in heat treatment for the as delivered condition of both batches the effect of micronotches in the notched surface region as well as the possible effect of residual stresses due to machining, as different machining parameters were used for the introduction of the notch geometries. However, these first results clearly demonstrate that in the VHCF regime the macroscopic notch effect does not solely dominate the fatigue behaviour as would have been expected from the LCF and HCF range.

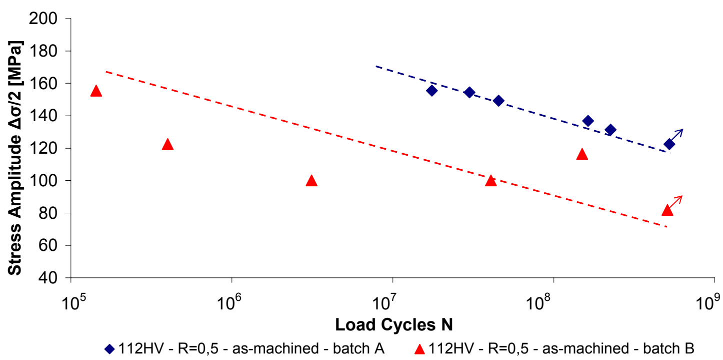

Fig. 5: Fatigue data for notched specimens of EN AW-6082, 112 HV, peak aged, R = 0,5, t = 1.

In figure 6 (a) the S-N data for smooth specimens of EN AW-6082 with 112 HV made of batch A and batch B are shown. In this case the tendency of fatigue behaviour in the VHCF regime is comparable for both batches, thus showing contradictory behaviour to the notched specimens. In Figure 6 (b) the S-N data of smooth specimens of EN AW-5083 H111 with 85 HV are given. A comparison with the S-N data of EN AW-6082 (figure 6 a) shows, that the much more ductile material EN AW-5083 shows a more pronounced scattering of fatigue data and failure occurs at lower stress amplitudes, as was expected for this alloy. The reason for the huge scattering could not yet be finally determined.

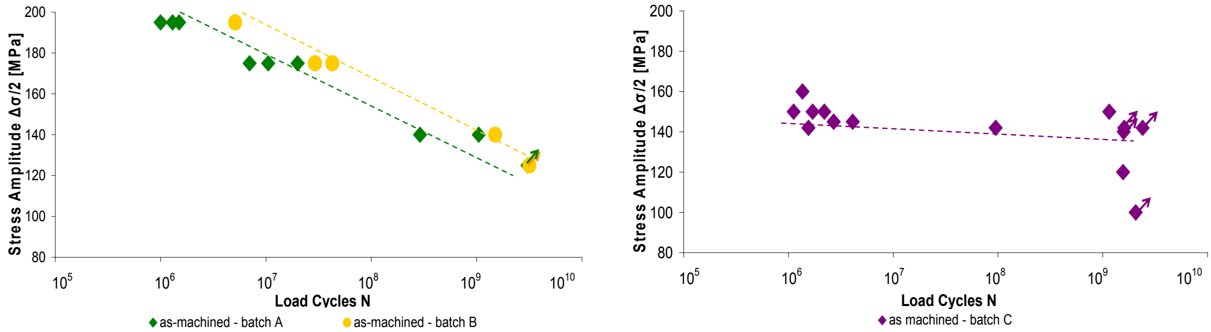

Fig. 6: (a) Fatigue data for smooth specimens EN AW-6082 and 112 HV and (b) fatigue data for smooth specimens EN AW-5083 and 85 HV

In Figure 7 the stress amplitudes of the notched and the smooth specimens are shown. The fatigue strength decreases tremendously for the specimens with the notch radius R = 0,5 made of batch B. The tendency of fatigue behaviour of the notched specimens of batch A is comparable to the smooth specimens (batch A).

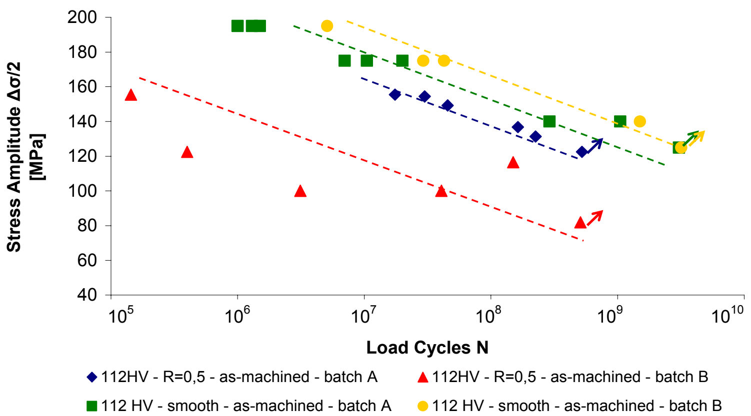

Fig. 7: Comparison of the notched with the smooth specimens, EN AW-6082 and 112 HV, as-machined.

The fracture surfaces of the failed fatigue specimens were examined by means of SEM. The crack initiation site for notched specimens was always at the surface. Figure 8 (a) shows a typical fracture surface of a notched specimen for $N_F = 4.5 \cdot 10^7$. The magnified area B shows the crack initiation at a micronotch due to the surface machining, encircled by the “feathered” structure of a fatigue fracture surface (area C), which is typical for this type of aluminium alloy. The remaining fracture surface consists of the typical dimpled structure indicating the final rupture (area A). Figure 8 (b) depicts a fracture surface of a smooth specimen of EN AW-6082 and 112 HV. The marked area D (Fig. 8c) shows the most likely crack initiation site. Hence, a possible change of the crack initiation from surface to a subsurface region must be taken into consideration with regard to further interpretations of the contradictory fatigue results for the different batches for notched and unnotched samples. This observed transition from surface to subsurface is in good agreement with B. Zettel et al. [3]. Fatigue tests at a stress ratio R ≠ -1 are planned in order to gain further insight into the crack initiating mechanisms.

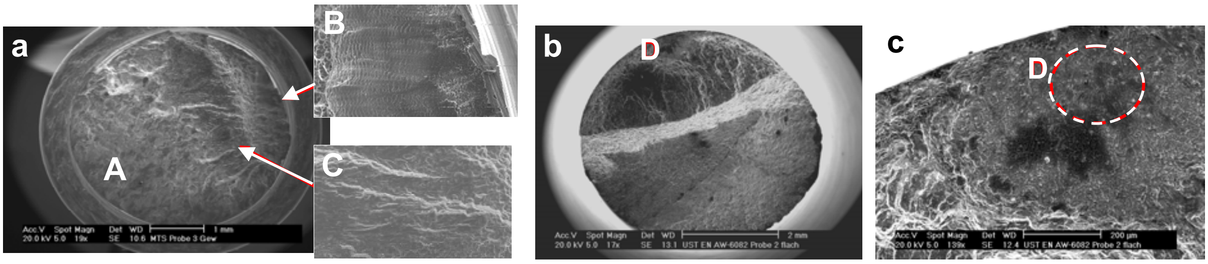

Fig. 8: (a) Typical fracture surface for notched specimen EN AW-6082 and 112 HV, as-machined (σ_a = 83 MPa, R = -1, $N_B = 4.5 \cdot 10^7$) and (b) fracture surface for smooth specimen EN AW-6082 and 112 HV, as-machined (σ_a = 175 MPa, R = -1, $N_B = 4.2 \cdot 10^7$) and (c) magnification of area D

CONCLUSION

With this study the first step towards a better understanding of the behaviour of welded aluminium alloys in the very high cycle fatigue regime was made. The different microstructures, inhomogeneities and the geometry of the welded seams of the work hardening aluminium alloy EN AW-5083 and the precipitation hardening aluminium alloy EN AW-6082 were characterized. Moreover the microscopic notch was mapped based on the measurement of strength gradients by means of Vickers microhardness. Based on these examinations the properties of the fatigue samples could be defined and first specimens could be manufactured. First fatigue results with samples representing the base material were obtained on with two different batches for the EN AW-6082. Despite similar notch geometry, surface quality and hardness the notched specimens out of batch A exposed a much higher cyclic strength in the VHCF regime than batch B. This different VHCF behaviour for two different batches of the EN AW-6082 alloy will have to be further analysed in the ongoing work. The SN-curves of batch A and B of smooth specimens of EN AW-6082 showed a rather similar behaviour. A comparison with the S-N data of EN AW-6082 shows that the much more ductile material EN AW-5083 exhibits a distinctly larger scattering of fatigue data and failure occurs at lower stress amplitudes, as was expected. However, the given fatigue results already indicate that the macroscopic notch does not solely define the fatigue behaviour as would have been expected from the HCF behaviour of welded structures. The examination of the fracture surfaces by means of SEM show always a crack initiation for the notched samples at the surface. A change of the crack initiation must be taken in consideration because of the change of crack initiation to a subsurface area for the smooth specimens. Further fatigue tests with a stress ratio R ≠ -1 are planned in order to get more information about the crack initiation site as well as the influence of mean stresses.

ACKNOWLEDGEMENT

The authors thank the Deutsche Forschungsgemeinschaft (DFG) for the financial support and are also indebted to Wieland Menn (ABUS Kransysteme GmbH) and Robert Lahnsteiner (MIG Weld GmbH) for the support of the welding trials.

REFERENCES

[1] H.-J Christ, M. Zimmermann, C. Stöcker, C. Müller-Bollenhagen
Aktuelle Fragestellungen, experimentelle Herausforderungen und neue Forschungsergebnisse zum Ermüdungsverhalten metallischer Werkstoffe im Bereich sehr hoher Lastspiele, in: Fortschritte der Kennwertermittlung für Forschung und Praxis, Herausgeber: M. Borsutzki und Stefanie Geisler, Verlag Stahleisen GmbH, Düsseldorf, (2009), pp. 7-14

[2] C. Berger, B. Pyttel, T. Trossmann
Very high cycle fatigue tests with smooth and notched specimens and screws made of light metal alloys, International Journal of Fatigue, No. 29, (2006), pp. 1640-1646.

[3] B. Zettl, S. Stanzl-Tschegg, H. Mayer
Crack initiation mechanisms and fatigue lifetime of AISI 420 steel under constant and variable Loading, Proceedings of the Fourth International Conference on Very High Cycle Fatigue (VHCF 4), ed. by J. E. Allison, J. Wayne Jones, J. M. Larsen, R. O. Ritchie, (2007), pp. 123-128.

[4] X. Zhu, A. Shyam, J. W. Jones, H. Mayer, J. V Lasecki, J. E. Allison
Elevated temperature fatigue behaviour of a 319 cast aluminium alloy in the gigacyle regime, Proceedings of the Third International Conference on Very High Cycle Fatigue – (VHCF 3), ed. by. T. Sakai, Y. Ochi, (2004), pp. 553-560.

[5] M. Zimmermann, H.-J. Christ
Influence of macroscopic and microscopic notch effects on the VHCF behaviour of a precipitation-hardened aluminium alloy, Proceedings of the Fourth International Conference on Very High Cycle Fatigue (VHCF 4), ed. by J. E. Allison, J. Wayne Jones, J. M. Larsen, R. O. Ritchie, (2007), pp. 295-301

[6] J. A. Collins
Failure of Materials in mechanical design
John Wiley & Sons Inc., New York, USA, (1981).

[7] B. Hänel, E. Haibach
Rechnerischer Festigkeitsnachweis für Maschinenbauteile
5. Edition, VDMA-Verlag, Frankfurt, (2003).

[8] N.-J. Ho; F. V. Lawrence
The Fatigue of weldments subjected to complex loadings
FCP Report No. 45, University of Illinois at Urbana-Champaign (1983).

[9] J.-Y. Yung, F. V. Lawrence
Analytical and graphical aids for the fatigue design of weldments
Fatigue Fracture Engineering Material Structure Vol. 8, No. 3, (1985), pp. 223-241.

Corresponding author: martin.cremer@uni-siegen.de